

GLUD1 supports ovarian cancer progression by counteracting anoikis via ARAF/MEK/ERK signaling

Received: 22 July 2025

Accepted: 19 February 2026

Cite this article as: Feng, H., Chen, Y., Wu, G. *et al.* GLUD1 supports ovarian cancer progression by counteracting anoikis via ARAF/MEK/ERK signaling. *npj Precis. Onc.* (2026). <https://doi.org/10.1038/s41698-026-01349-6>

Huolun Feng, Yanzen Chen, Geyan Wu, Zhentao Zhang, Hongkun Lai, Changnian Yang, Shaofen Zhang, Yongqing Lin, Yingqi Liu, Haiyan Ye, Shanshan Wu & Lixue Cao

We are providing an unedited version of this manuscript to give early access to its findings. Before final publication, the manuscript will undergo further editing. Please note there may be errors present which affect the content, and all legal disclaimers apply.

If this paper is publishing under a Transparent Peer Review model then Peer Review reports will publish with the final article.

**GLUD1 Supports Ovarian Cancer Progression by Counteracting Anoikis via
ARAF/MEK/ERK Signaling**

Huolun Feng^{#1,2}, Yanzhen Chen^{#3}, Geyan Wu^{#4}, Zhentao Zhang⁵, Hongkun Lai², Changnian Yang⁵,
Shaofen Zhang³, Yongqing Lin³, Yingqi Liu⁵, Haiyan Ye^{*3}, Shanshan Wu^{*6}, Lixue Cao^{*7}

1. Guangdong Cardiovascular Institute, Guangdong Provincial People's Hospital (Guangdong Academy of Medical Sciences), Guangzhou, Guangdong, China
2. Department of Gastrointestinal Surgery, Department of General Surgery, Guangdong Provincial People's Hospital (Guangdong Academy of Medical Sciences), Southern Medical University, Guangzhou, China.
3. Department of Gynecology, Guangdong Provincial People's Hospital, Guangdong Academy of Medical Sciences, Southern Medical University, Guangzhou, Guangdong, China.
4. Biomedicine Research Centre, The Third Affiliated Hospital of Guangzhou Medical University, Guangzhou Medical University, Guangzhou, China.
5. The First Clinical College, Guangdong Medical University, Zhanjiang, Guangdong, China
6. Department of Biology, School of Basic Medical Science, Guangdong Medical University, Zhanjiang, Guangdong, China
7. Medical Research Institute, Guangdong Provincial People's Hospital (Guangdong Academy of Medical Sciences), Southern Medical University, Guangzhou, Guangdong, China

Contributed equally.

* Correspondences should be addressed to: Lixue Cao, caolixue@gdph.org.cn; Shanshan Wu, wushsh@gdmu.edu.cn; Haiyan Ye, yehaiyan@gdph.org.cn.

Abstract:

Peritoneal dissemination is the major cause of mortality in epithelial ovarian cancer (EOC) and requires tumor cells to survive in a detached state by evading anoikis. However, the molecular mechanisms supporting anchorage-independent survival remain poorly defined. Here, we identify glutamate dehydrogenase 1 (GLUD1) as a key regulator of anoikis resistance and metastatic progression in EOC. GLUD1 expression was elevated in metastatic EOC tissues and associated with unfavorable clinical outcomes. Loss of GLUD1 impaired anoikis resistance and reduced metastatic capacity of ovarian cancer cells in vitro, while markedly suppressing peritoneal dissemination and prolonging survival in vivo. Mechanistically, GLUD1 was found to interact with a key protein ARAF, the A-Raf proto-oncogene. By limiting ubiquitin–proteasome-mediated degradation of ARAF, GLUD1 exerted a non-enzymatic function that stabilized ARAF protein levels and sustained MEK/ERK signaling. Together, these findings reveal a non-canonical role of GLUD1 in regulating protein stability and identify the GLUD1–ARAF axis as a critical mechanism supporting anchorage-independent survival during peritoneal dissemination of EOC.

Keyword: Anoikis, Metastasis, Ovarian cancer, GLUD1

Introduction

According to GLOBOCAN 2020, ovarian cancer remains the most lethal gynecologic malignancy, with epithelial ovarian cancer (EOC) accounting for the majority of cases and deaths¹. Its high mortality is largely attributed to extensive peritoneal metastasis and the presence of malignant ascites at diagnosis². Within malignant ascites, EOC cells aggregate in suspension and survive in an anchorage-independent manner by evading anoikis, a form of programmed cell death triggered by detachment from the extracellular matrix (ECM)^{3,4}. Although anoikis resistance is essential for metastatic dissemination, the molecular mechanisms that sustain the survival of detached EOC cells remain incompletely understood.

Metabolic reprogramming has emerged as a key adaptive strategy that enables cancer cells to evade anoikis and support metastatic progression^{5,6}. Alterations in glycolysis, amino acid metabolism, and lipid metabolism collectively meet the energetic and biosynthetic demands of detached tumor cells^{7,6,8}. Increasing evidence suggests that glutamine metabolism contributes to the maintenance of tricarboxylic acid (TCA) cycle activity under anchorage-independent conditions, underscoring the metabolic flexibility required for survival during detachment^{6,9,10}. Glutamate dehydrogenase 1 (GLUD1), a key enzyme in glutamine metabolism, catalyzes the conversion of glutamate to α -ketoglutarate (α -KG), supporting TCA cycle replenishment to meet the energy and biosynthetic needs of detached tumor cells¹¹⁻¹⁵. However, the specific role of GLUD1 in anoikis resistance and metastatic progression of EOC remains poorly defined.

In this study, we integrated transcriptomic datasets with curated gene signatures related to anoikis and amino acid metabolism and identified GLUD1 as a candidate gene associated with metastatic progression. GLUD1 expression was markedly elevated in metastatic EOC tissues and correlated with shorter overall and disease-free survival. Functional studies demonstrated that GLUD1 critically promotes anoikis resistance and metastasis *in vitro* and *in vivo*. Notably, our findings reveal that GLUD1 exerts a previously unrecognized non-enzymatic regulatory function by modulating the stability of the RAF family kinase ARAF, thereby sustaining MEK–ERK signaling under detachment conditions. These results reveal an unappreciated mechanism through which GLUD1 contributes to anchorage independent survival and provide new insight into the metastatic biology of EOC.

Results

GLUD1 is identified as an anoikis- and amino acid metabolism–related gene in EOC

To identify key regulators in ovarian cancer, we performed a comprehensive analysis of three publicly available gene expression datasets (GSE26712, GSE27651, and GSE40595; total $n = 278$). Differentially expressed genes (DEGs) between EOC tissues and controls were identified using predefined statistical criteria with criteria of false discovery rate (FDR) < 0.05 and $|\log_2FC| \geq 0.7$ (Figure 1A). These genes were subsequently intersected with curated gene sets related to anoikis and amino acid metabolism. Among all candidates, GLUD1 was the only gene present in both functional gene sets (Figure 1B). Other genes, such as GLS2, SLC1A5, and SLC7A5, were found in only one of the two functional gene sets and were therefore not pursued further. Analysis revealed that GLUD1 expression was significantly upregulated in ovarian cancer tissues compared to normal controls (GSE27651, $p < 0.001$, Figure 1C). Furthermore, Kaplan–Meier survival analysis demonstrated that elevated GLUD1 expression was significantly associated with worse overall survival (OS) and progression-free survival (PFS) in EOC patients (TCGA-OV, $n = 420$, $P = 0.008$; KM-plotter, $n = 373$, $p = 0.0045$; KM-plotter, $n = 177$, $p = 0.044$; Figure 1D and Supplemental Figure 1A).

Further stratified analysis revealed that the inverse association between GLUD1 expression and progression-free survival was significant in patients with advanced-stage disease (stage III/IV), whereas no significant association was observed in early-stage patients (stage I/II) (KM-plotter OV-I/II, $n = 163$, $p = 0.27$; OV-III/IV, $n = 1081$, $p = 0.049$; Supplementary Figure 1B).

Collectively, these analyses identify GLUD1 as a gene associated with anoikis, amino acid metabolism, and unfavorable prognosis in advanced-stage epithelial ovarian cancer.

GLUD1 expression is elevated in metastatic EOC and correlates with poor clinical outcomes

Based on a screening of GLUD1 protein expression, we chose the OVCAR3 and SKOV3 ovarian cancer cell lines for subsequent experiments. (Supplemental Figure 2). To assess whether GLUD1 expression is regulated during anoikis, OVCAR3 and SKOV3 cells were cultured under detached conditions. GLUD1 protein levels increased progressively during suspension culture, consistent with a potential role in anoikis resistance (Figure 1E).

In view of the results, immunohistochemical analysis was performed on the clinical specimens of ovarian cancer. It was found that GLUD1 expression was significantly higher in metastatic epithelial ovarian cancer tissues than in primary tumors and adjacent non-tumor tissues (Figure 1F). Based on immunohistochemical scoring, patients were stratified into GLUD1_{high} and GLUD1_{low} groups. Kaplan–Meier analysis revealed that high GLUD1 expression was associated with shorter overall survival ($p = 0.002$) and disease-free survival ($p = 0.02$) (Figure 1G). Clinical correlation analysis showed that GLUD1 expression was significantly associated with patients' vital status, with a higher proportion of deaths in the high-expression group (Supplemental Table 1). Both univariate and multivariate Cox regression analyses identified GLUD1 as an independent risk factor for overall survival (Supplementary Table 2). Together, these findings indicate that GLUD1 expression is elevated in metastatic epithelial ovarian cancer and correlates with adverse clinical outcomes.

GLUD1 Dysregulation Drives Anoikis Resistance and Migration in EOC Cells

To investigate the functional role of GLUD1 in epithelial ovarian cancer, stable GLUD1-overexpressing and GLUD1-silenced OVCAR3 and SKOV3 cell lines were established (Figure 2A). Under suspension culture conditions, GLUD1 knockdown resulted in a time-dependent reduction in spheroid size and proliferative capacity (Supplementary Figure 3). Calcein-AM/PI staining demonstrated that GLUD1 overexpression reduced apoptosis, whereas GLUD1 silencing caused a significant, time-dependent increase in apoptosis under detached conditions (Figure 2B). These results were corroborated by Annexin V–FITC/PI flow cytometry analysis, which similarly showed that GLUD1 overexpression suppressed, while GLUD1 knockdown enhanced, anoikis in suspension cultures (Figure 2C).

Given the established link between anoikis resistance and metastatic dissemination, we next examined whether GLUD1 influences cell migration. Gene set enrichment analysis revealed that GLUD1 expression positively correlated with gene signatures associated with migration and metastasis (Supplementary Figure 4A). Consistently, GLUD1 overexpression enhanced, whereas GLUD1 knockdown impaired, the migratory capacity of epithelial ovarian cancer cells in both Transwell and wound-healing assays (Figure 2D–E). These findings demonstrate that GLUD1 promotes anoikis resistance and migratory behavior in epithelial ovarian cancer cells.

Knockdown of GLUD1 suppressed peritoneal dissemination *in vivo*

To further investigate the *in vivo* biological role of GLUD1, a mouse model of intraperitoneal ovarian cancer implantation was established (Figure 3A). Survival analysis revealed that GLUD1 inhibition significantly prolonged the survival of tumor-bearing mice compared to the control group (Figure 3B). Upon necropsy, a notable reduction in metastatic nodules in the spleen, liver, and peritoneal cavity was observed in the GLUD1-silenced group (Figure 3C-D). Histological analysis of abdominal tumor tissues, including Hematoxylin and Eosin (H&E) and TUNEL staining, demonstrated that tumors derived from GLUD1-silenced cells exhibited a higher proportion of apoptotic cells (Figure 3E-F). Immunohistochemistry (IHC) further confirmed reduced GLUD1 expression, and importantly, a decrease in Ki-67 staining, indicating reduced proliferative activity in the GLUD1 knockdown group (Figure 3E-F). Collectively, these *in vivo* results demonstrate that GLUD1 suppression inhibits tumor growth, survival, and peritoneal dissemination in ovarian cancer.

GLUD1 interacts with and stabilizes ARAF to activate MEK–ERK signaling

GSEA analysis revealed that GLUD1 expression is positively associated with RAF activation and ERK/MAPK signaling pathways (Supplementary Figure 4B). To elucidate the molecular mechanisms underlying GLUD1 function in ovarian cancer cells, IP-MS was performed in OVCAR3-GLUD1-overexpressing cells, leading to the identification of GLUD1-interacting proteins (Figure 4A). Among the specific interactors, ARAF was identified as a binding partner of GLUD1, and is known to modulate survival signaling (Figure 4B). We further performed immunoprecipitation (IP) assays to evaluate the interaction between GLUD1 and ARAF. The result showed that GLUD1 is bound to ARAF (Figure 4C). Subcellular localization analyses showed that ARAF predominantly co-localizes with GLUD1 in the cytoplasm, with only a minor fraction in mitochondria (Figure 4D). Interestingly, knockdown of GLUD1 led to a pronounced reduction in ARAF protein levels, whereas BRAF and CRAF expression remained unaffected and neither interacted with GLUD1 (Figure 4E and Supplementary 5A-B). Given that ARAF is reported to activate the MEK/ERK pathway and modulate apoptosis in cancer cells, we next examined this signaling axis. Western blot confirmed that GLUD1 knockdown significantly inhibited ARAF levels and phosphorylation of MEK and ERK. Concomitantly, expression of the anti-apoptotic protein BCL-2 decreased, whereas levels of BIM and cleaved caspase-3 increased (Figure 4E). Moreover, re-expression of ARAF restored ERK phosphorylation in cells with

GLUD1 knockdown (Figure 4F). Consistently, under suspension conditions, cells with higher GLUD1 levels exhibited a time-dependent increase in ARAF and p-ERK, indicating an adaptive survival response activated to counteract ongoing anoikis stress (Figure 4G). Collectively, these results suggest that GLUD1 specifically stabilizes ARAF and promotes downstream MEK/ERK signaling to regulate cell survival.

GLUD1 Stabilizes ARAF by Suppressing Ubiquitin–Proteasome–Mediated Degradation

To further investigate the mechanism by which GLUD1 regulates ARAF expression, we examined whether ARAF protein stability is controlled by proteasomal degradation. Treatment with the proteasome inhibitor MG132 reversed the reduction of ARAF protein levels induced by GLUD1 knockdown, indicating that GLUD1 regulates ARAF at the post-translational level (Figure 5A). Consistently, cycloheximide chase assays revealed that the half-life of ARAF was significantly shortened in GLUD1-silenced cells compared with control cells (Figure 5B). To determine whether ubiquitin–proteasome–mediated degradation underlies GLUD1-dependent ARAF stabilization, ubiquitination assays were performed. Ubiquitination assays revealed decreased polyubiquitination of ARAF upon GLUD1 overexpression, supporting a role for the ubiquitin–proteasome pathway in this process (Figure 5C). To functionally validate this regulatory relationship, ARAF was reintroduced into GLUD1-silenced ovarian cancer cells. Re-expression of ARAF partially rescued the increased apoptosis observed under detached conditions following GLUD1 knockdown (Figure 5D). In addition, Transwell migration assays demonstrated that ARAF re-expression restored the impaired migratory capacity induced by GLUD1 depletion (Figure 5E). Collectively, these results indicate that GLUD1 promotes anoikis resistance and metastatic behavior in ovarian cancer cells by stabilizing ARAF protein.

Clinical correlation of GLUD1 and ARAF expression in EOC

To validate the relevance of the GLUD1–ARAF axis in clinical specimens, GLUD1 and ARAF protein expression was examined in epithelial ovarian cancer tissues. Immunohistochemical analysis revealed a significant positive correlation between GLUD1 and ARAF expression levels (Figure 6A). This association was further confirmed in freshly collected ovarian cancer specimens, which exhibited concordant expression patterns of GLUD1 and ARAF (Figure 6B). Collectively, these findings support a model in which GLUD1 promotes anoikis resistance and

metastatic progression in epithelial ovarian cancer through stabilization of ARAF and activation of downstream MEK–ERK signaling (Figure 6C).

ARTICLE IN PRESS

Discussion:

Detached EOC cells encounter significant metabolic and signaling stress within malignant ascites, and their ability to evade anoikis is therefore essential for successful peritoneal dissemination¹⁻³. This biological context underscores the need to define the molecular processes that permit anchorage-independent survival. In this study, we identify GLUD1 as a determinant of anoikis resistance in EOC. GLUD1 expression is elevated in metastatic tissues, correlates with unfavorable clinical outcomes, and is required for the survival and dissemination of detached tumor cells. Together, these findings address an important knowledge gap regarding the mechanisms that sustain epithelial ovarian cancer cell viability during transcoelomic spread and reveal a link between amino acid metabolism-associated genes and survival signaling in this setting.

Accumulating evidence indicates that GLUD1 can influence oncogenic signaling pathways, suggesting that its biological functions may extend beyond canonical metabolic regulation¹¹⁻¹⁵. For example, GLUD1 promotes metastasis of EGFR-activated lung cancer through activation of cAMP response element-binding protein (CREB) signaling¹⁵, and α -ketoglutarate generated by GLUD1 suppresses H3K27 methylation, leading to upregulation of PDPK1 and activation of the PI3K/AKT/mTOR pathway¹⁴. Despite these observations, the mechanisms by which GLUD1 regulates survival signaling in epithelial ovarian cancer have remained unclear. In this study, using immunoprecipitation–mass spectrometry followed by co-immunoprecipitation validation, we identify ARAF as a novel binding partner of GLUD1. This interaction enhances ARAF protein stability, thereby activating MEK/ERK signaling and promoting anoikis resistance and metastatic behavior in ovarian cancer cells.

GLUD1 has been classically characterized as a metabolic enzyme that catalyzes the conversion of glutamate to α -ketoglutarate, thereby regulating glutaminolysis and influencing tumor cell proliferation, apoptosis, and metastasis^{11,12,14,15}. Consistent with this enzymatic role, our data show that α -ketoglutarate supplementation partially restores ARAF abundance and ERK activity (Supplementary Figures 6A–B)). However, the incomplete rescue indicates that GLUD1-

mediated regulation of ARAF cannot be fully explained by its catalytic activity alone. These findings support a non-enzymatic role for GLUD1 in sustaining survival signaling under detachment conditions. In line with this concept, GLUD1 has recently been reported to exert non-catalytic regulatory functions through protein–protein interactions, including binding to the autophagy adaptor p62 (SQSTM1) to promote tumor cell survival under metabolic stress¹⁶. Thus, GLUD1 regulates the ARAF–MEK–ERK axis through both enzymatic and non-enzymatic mechanisms, with protein stabilization representing the dominant mode of action in detached ovarian cancer cells.

Within the canonical RAS–RAF–MEK–ERK signaling cascade, the RAF kinases ARAF, BRAF, and CRAF serve as central regulators of cell proliferation, differentiation, and survival¹⁷⁻¹⁸. The stability and integrity of RAF proteins are tightly controlled and are essential for signaling fidelity²⁰⁻²³. Although HSP90 is a well-established chaperone required for stabilization of RAF family kinases²⁰, overexpression of HSP90 did not rescue the reduction in ARAF protein levels caused by GLUD1 depletion (Supplementary Fig. 7A). Instead, silencing GLUD1 selectively reduced ARAF protein abundance without affecting BRAF or CRAF, indicating that GLUD1 stabilizes ARAF at the post-translational level through an HSP90-independent mechanism. Consistently, GLUD1 depletion shortened the half-life of ARAF and increased its ubiquitination, supporting a model in which GLUD1 limits ubiquitin–proteasome–mediated degradation of ARAF. Moreover, restoration of ARAF expression in GLUD1-deficient cells partially rescued anoikis resistance under detachment conditions and restored migratory capacity, providing functional evidence that ARAF stabilization is a key downstream effector of GLUD1-mediated survival and metastatic behavior. In addition, GLUD1 depletion did not appreciably alter FAK, AMPK, or CREB signaling, suggesting that these pathways are unlikely to play dominant roles in GLUD1-regulated anoikis resistance (Supplementary Fig. 7B). Collectively, these data support a specific, post-translational, and HSP90-independent role for GLUD1 in maintaining ARAF stability and downstream ERK signaling.

Functionally, the GLUD1–ARAF–MEK/ERK axis confers a survival advantage to detached ovarian cancer cells by suppressing anoikis and facilitating metastatic progression. The prominence of this regulatory mechanism under suspension conditions highlights a context-specific requirement for ARAF-dependent ERK signaling during transcoelomic dissemination. The clinical relevance of this axis is further supported by the positive correlation between GLUD1 and ARAF expression observed in epithelial ovarian cancer specimens. However, due to the relatively limited patient sample size, it is necessary to validate these findings in larger, multicenter independent patient cohorts in future studies. Collectively, these findings identify GLUD1 as a previously unrecognized modulator of ARAF and establish a mechanistic link between glutamine metabolism and RAF–MEK–ERK signaling in epithelial ovarian cancer. Beyond its mechanistic significance, identification of the GLUD1–ARAF–MEK/ERK axis also raises the possibility of therapeutic intervention in epithelial ovarian cancer. Pharmacologic inhibition of GLUD1, including agents such as R162, as well as clinically available MEK or ERK inhibitors, may disrupt the detachment-survival program that drives peritoneal metastasis^{11, 24}. However, GLUD1 is a central metabolic enzyme, and its dual metabolic and non-enzymatic functions introduce important complexity for therapeutic targeting. An unresolved question is how GLUD1 coordinates its enzymatic and non-enzymatic activities in different cellular contexts, and under what conditions each function predominates. Although our data support a role for GLUD1 in ARAF stabilization that cannot be fully explained by its metabolic output alone, the molecular mechanisms that govern the balance between GLUD1's catalytic and non-canonical scaffolding functions remain to be defined. Further studies will be required to elucidate the regulatory cues, subcellular compartmentalization, or interaction networks that determine GLUD1 functional engagement in ovarian cancer.

Methods

In silico analysis

Relevant datasets were retrieved from the Gene Expression Omnibus (GEO) database (<http://www.ncbi.nlm.nih.gov/geo/>). Based on these criteria, three datasets (GSE26712, GSE27651, and GSE40595) were selected for further analysis. Differential expression analysis was conducted using the limma package in R (v3.46.0), applying thresholds of $|\log_2FC| > 0.7$ and $(FDR) < 0.05$. In addition, volcano plots were generated to visualize gene distribution based on statistical significance and fold change, enabling intuitive comparison of expression patterns. A total of 422 anoikis-related genes and 709 amino acid metabolism-related genes were retrieved from published literature²⁵. We performed intersection analysis using Venn diagrams to identify the overlapping genes, which are considered core genes involved in both anoikis and amino acid metabolism. Kaplan–Meier analysis (<https://kmplot.com>) was used to assess the prognostic significance in ovarian cancer.

Clinical tissue specimens

Ovarian cancer tissues were collected from 60 epithelial ovarian cancer (EOC) patients at Guangdong Provincial People's Hospital. Written informed consent was obtained from all participants, and the study was approved by the Ethics Committee of Guangdong Provincial People's Hospital (Approval No. KY-Z-2020-518-03), in accordance with the Declaration of Helsinki. In addition, formalin-fixed, paraffin-embedded ovarian cancer tissue microarrays (TMAs) were obtained from the National Engineering Center for Biochip (Outdo Biotech, Shanghai, China). Use of these TMAs was approved by the Outdo Biotech Clinical Research Ethics Committee (Approval No. SHYJS-CP-1804029). Informed consent for TMA samples was obtained by the provider or waived due to the use of anonymized archival specimens, in accordance with institutional guidelines. The TMAs included 4 cases of adjacent non-tumor tissue, 134 cases of primary ovarian cancer, and 12 cases of metastatic tumors. Corresponding clinical information is provided in Supplementary Table 1.

Cell culture

The human embryonic kidney cell line HEK293T and human ovarian cancer cell lines SKOV3, OVCAR3, HO8910PM, ES-2, A2780, and Caov-3 were obtained from the American Type

Culture Collection (ATCC, Manassas, VA, USA). Cells were cultured in Dulbecco's Modified Eagle Medium (DMEM; GIBCO) supplemented with 10% fetal bovine serum (FBS; ExCell) and 1% penicillin-streptomycin. All cells were maintained at 37°C in a humidified incubator with 5% CO₂.

Lentiviral transduction and plasmid transfection

Lentiviral vectors encoding full length GLUD1 or short hairpin RNAs targeting GLUD1 were co-transfected with packaging plasmids (psPAX2 and pMD2.G) into HEK293T cells to generate lentiviral particles. Viral supernatants were collected 48 hours after transfection, filtered, and concentrated as needed. OVCAR3 and SKOV3 cells were infected with the lentiviruses in the presence of polybrene (8 µg/mL), followed by puromycin selection (1 µg/mL) to establish stable GLUD1-overexpressing and GLUD1-silenced cell lines. The shRNA targeting sequence for GLUD1 was GCTACCTGGGCGAAGCGCTGT. In addition, plasmids encoding full-length ARAF and HSP90 were purchased from the MiaoLing Plasmid Platform and transfected into cells as indicated.

Anoikis induction

Anoikis was induced by culturing cells in ultra-low attachment plates. Cells were harvested, washed, and seeded in serum containing medium under suspension conditions for the indicated time points. Cells cultured on standard tissue culture plates were used as attached controls.

Cell viability and apoptosis assays

Cell viability under detached conditions was assessed using Calcein AM and propidium iodide staining according to the manufacturer's instructions. Apoptosis was further quantified using Annexin V FITC and propidium iodide staining followed by flow cytometry analysis. For all assays, three independent biological replicates were performed.

Immunofluorescence microscopy

Cells grown on glass coverslips were incubated with 100 nM MitoTracker Deep Red (Invitrogen) for 20 minutes at 37 °C. After staining, cells were fixed with paraformaldehyde, permeabilized, and blocked in PBS containing 5% BSA. Cells were then incubated with primary antibodies against GLUD1 (mouse, 1:200) and ARAF (rabbit, 1:200), followed by Alexa Fluor 488–

conjugated anti-mouse IgG and Alexa Fluor 555–conjugated anti-rabbit IgG secondary antibodies (1:500), each for 1 hour at room temperature. Nuclei were counterstained with DAPI, and coverslips were mounted using antifade mounting medium. Images were acquired using a confocal fluorescence microscope.

Western Blot Analysis

Western blotting was performed using primary antibodies from multiple sources. Antibodies against GLUD1 (1:1000, Cat# 14299-1-AP), GAPDH (1:5000, Cat# 60004-1-Ig), MEK (1:1000, Cat# 11049-1-AP), BRAF (1:1000, Cat# 20899-1-AP) antibody, CRAF (1:1000, Cat# 66592-1-Ig) antibody, HSP90(1:1000, Cat# 13171-1-AP) antibody, and Flag-tag (1:1000, Cat# 20543-1-AP) were obtained from Proteintech Group (Chicago, IL, USA). Antibodies against phospho-MEK (p-MEK) (1:1000, Cat# 9154T), ERK (1:1000, Cat# 4695T), phospho-ERK (p-ERK) (1:1000, Cat# 4370T), BIM(1:1000, Cat# 2933T) antibody, cl-caspase 3(1:1000, Cat# 9664S) antibody, FAK(1:1000, Cat# 3285T) antibody, p-FAK(1:1000, Cat# 8556T) antibody, AMPK(1:1000, Cat# 5831T) antibody, p-AMPK(1:1000, Cat# 2535T) antibody, CREB(1:1000, Cat# 9197T) antibody, p-CREB(1:1000, Cat# 9198T), and BCL-2 (1:1000, Cat# 15071T) were purchased from Cell Signaling Technology (Danvers, MA, USA). The ARAF antibody (1:1000, Cat# ab200653) was obtained from Abcam (Cambridge, UK). antibody IRDye® 800CW Goat anti-Rabbit IgG (1:5000, Cat# 926-32211) and IRDye® 680RD Goat anti-Mouse IgG (1:5000, Cat# 926-68070) secondary antibodies were purchased from LI-COR Biosciences (Lincoln, NE, USA). Protein bands were visualized using the Odyssey CLx Imaging System and quantified with Image Studio Lite software (version 4.0; LI-COR Biosciences).

Co-immunoprecipitation (Co-IP) Assay

Co-IP assays were performed as previously described. Briefly, cells were lysed in IP lysis buffer supplemented with a protease inhibitor cocktail. The total lysates were incubated overnight at 4°C with pre-conjugated magnetic beads (MedChemExpress, USA) on a rotating wheel. The following day, supernatants were carefully removed using a magnetic stand, and the protein-bound beads were washed six times with wash buffer. Proteins were eluted by adding loading buffer and heating at 100°C for 10 minutes, followed by immunoblotting analysis.

Ubiquitination Assay

OVCAR3 and SKOV3 cells were transfected with plasmids expressing Myc-ARAF, Flag-ubiquitin (Flag-Ub), and GLUD1 as indicated. Cells were treated with MG132 (20 μ M) for 6 hours to inhibit proteasomal degradation and allow ubiquitinated proteins to accumulate. Cell lysates were prepared and subjected to immunoprecipitation using an anti-Myc antibody to pull down Myc-ARAF. The immunoprecipitants were then analyzed by western blotting with an anti-Flag antibody to detect ubiquitinated ARAF.

Immunohistochemistry and TUNEL staining

Tissue sections were processed and stained according to standard protocols at the Biopathology Institute (Servicebio, Wuhan, Hubei, China) using primary antibodies against GLUD1 (1:1000), ARAF (1:100), and Ki-67 (1:200). Immunostaining intensity was scored as follows²⁶: negative (0), weak (1), moderate (2), and strong (3). The extent of staining was evaluated based on the percentage of positively stained cells: 0 (<10%), 1 (10%–25%), 2 (25%–50%), 3 (50%–75%), and 4 (>75%). In the xenograft mouse model, mice were sacrificed by cervical dislocation. Tumors were excised, fixed in 4% formaldehyde, embedded in paraffin, and subjected to hematoxylin and eosin (H&E) staining at the Biopathology Research Institute (Servicebio). Images of H&E-stained sections were captured using a Leica DM6B microscope (Leica, Wetzlar, Hessen, Germany). Apoptosis in tumor tissues was assessed using a TUNEL assay kit according to the manufacturer's instructions, and apoptotic indices were calculated as the percentage of TUNEL positive cells.

Cell migration assays

Cell migration was evaluated using Transwell chambers and wound healing assays. For Transwell assays, cells were seeded into the upper chamber in serum free medium, and medium containing 10 percent fetal bovine serum was added to the lower chamber as a chemoattractant. After incubation, migrated cells were fixed, stained, and quantified. Wound healing assays were performed by creating a linear scratch and monitoring wound closure over time. All migration assays were performed in three independent experiments.

Intracellular Metabolite Measurements

Intracellular α -KG levels were quantified using a commercial α -ketoglutarate assay kit (Sigma-Aldrich) following the manufacturer's instructions. Briefly, 2×10^6 cells were homogenized in

PBS, and the supernatant was collected after centrifugation. Proteins were removed using 10-kDa Amicon Ultra centrifugal filters (Millipore), and the resulting flow-through containing small metabolites was used for α -KG measurement.

Animal experiments

Xenograft tumor experiments were approved by the Institutional Animal Care and Use Committee of Guangdong Provincial People's Hospital (Guangdong Academy of Medical Sciences, Southern Medical University; Approved No.KY-Z-2020-518-03). To ensure adequate statistical power, six female BALB/c-nu mice (6 weeks old) were used per group, and mice were randomly assigned to experimental groups²⁷⁻²⁹. For the intraperitoneal metastasis model, a single-cell suspension containing 2×10^6 cells was injected into the peritoneal cavity of BALB/c-nu mice. In survival studies, mice that met predefined endpoint criteria such as sustained weight loss, respiratory distress, or irreversible recumbency were euthanized by cervical dislocation without anesthesia, in accordance with institutional animal care guidelines. Tumors were harvested and fixed in paraformaldehyde. Visible tumor nodules were counted and fixed tumor tissues were subsequently embedded in paraffin, sectioned, and stained with hematoxylin and eosin (H&E) for histological analysis.

Statistical analysis

Functional analysis was performed using the SPSS software package (version 24.0, IBM SPSS, IL, USA) and GraphPad Prism (version 8.0, GraphPad Software, CA, USA). We used Student's t-test to examine the difference in means between two groups, and One-way ANOVA to examine the difference between multiple groups. A Chi-square test was used for correlation analysis between gene expression and clinicopathological features. The Kaplan-Meier method was used to test the overall survival between different groups. A p value < 0.05 was considered a statistically significant difference.

Acknowledgements:

This work was also supported by the Guangdong Basic and Applied Basic Research Foundation (2025A1515012496, 2022A1515010243), Guangzhou Municipal Science and Technology Project (2024A04J3475), College Students' Innovative Entrepreneurial Training Plan Program (S202510571044) and Special Funds for the Cultivation of Guangdong College Students' Scientific and Technological Innovation(No.pdjh2025bk102). We would like to express our gratitude to these funding sources for their support.

Data Availability Statement:

All data supporting the findings of this study are presented in the article and the Supplementary Materials. Our study does not generate any new datasets. The datasets presented in this study can be found from the following links: TCGA (<https://portal.gdc.cancer.gov/>), GSE26712, GSE27651 GSE40595. All other raw data are available upon reasonable request from the corresponding author.

Code Availability Statement:

The methods described in this manuscript have been used the public available limma package in R (v3.46.0) for differential gene expression analysis. No custom algorithm generated in this manuscript.

Competing Interests:

The authors declare that they have no competing interests.

Author Contributions:

LC, HF and GW designed experiments. ZZ performed the bioinformatics analysis. YC, HL, YL, SZ, YL and CY performed the experiments and analyzed and interpreted the data. HY, SW and

LC supported and supervised the research. LC and HF wrote the manuscript, and all authors read and approved the final manuscript. All authors read and approved the final manuscript.

ARTICLE IN PRESS

References:

1. Cabasag, C. J. et al. Ovarian cancer today and tomorrow: A global assessment by world region and human development index using GLOBOCAN 2020. *Int. J. Cancer* 151, 1535–1541 (2022).
2. Lin, S.-C. et al. Periostin promotes ovarian cancer metastasis by enhancing M2 macrophages and cancer-associated fibroblasts via integrin-mediated NF- κ B and TGF- β 2 signaling. *J. Biomed. Sci.* 29, 109 (2022).
3. Saha, M. et al. Sustained AMPK activation and proline metabolism play critical roles in the survival of matrix-deprived transformed cells. *Front. Cell Dev. Biol.* 9, 771366 (2021).
4. Davison, C. A. et al. Antioxidant enzymes mediate survival of breast cancer cells deprived of extracellular matrix. *Cancer Res.* 73, 3704–3715 (2013).
5. Shaw, P. et al. Anoikis resistance in cancer: Mechanisms, therapeutic strategies, potential targets, and models for enhanced understanding. *Cancer Lett.* 624, 217750 (2025).
6. Endo, H. et al. Metabolic reprogramming sustains cancer cell survival following extracellular matrix detachment. *Redox Biol.* 36, 101643 (2020).
7. Zhu, C. et al. Adipose-derived stem cells promote glycolysis and peritoneal metastasis via TGF- β 1/SMAD3/ANGPTL4 axis in colorectal cancer. *Cell. Mol. Life Sci.* 81, 189 (2024).
8. Li, S. et al. Obesity promotes gastric cancer metastasis via diacylglycerol acyltransferase 2-dependent lipid droplets accumulation and redox homeostasis. *Redox Biol.* 36, 101596 (2020).
9. Sullivan, L. B. et al. Supporting aspartate biosynthesis is an essential function of respiration in proliferating cells. *Cell* 162, 552–563 (2015).
10. Altman, B. J. et al. From Krebs to clinic: Glutamine metabolism to cancer therapy. *Nat. Rev. Cancer* 16, 749–764 (2016).
11. Jin, L. et al. The PLAG1–GDH1 axis promotes anoikis resistance and tumor metastasis through CamKK2–AMPK signaling in LKB1-deficient lung cancer. *Mol. Cell* 69, 87–99.e7 (2018).
12. Yang, R. et al. EGFR activates GDH1 transcription to promote glutamine metabolism through the MEK/ERK/ELK1 pathway in glioblastoma. *Oncogene* 39, 2975–2986 (2020).
13. Wang, X. et al. α -Ketoglutarate-activated NF- κ B signaling promotes compensatory glucose uptake and brain tumor development. *Mol. Cell* 76, 148–162.e7 (2019).
14. Yang, R. et al. GDH1-catalytic glutaminolysis feedback activates EGFR/PI3K/AKT pathway and reprograms glioblastoma metabolism. *Neuro-Oncology* 26, noae222 (2024).

15. Kang, J. et al. EGFR-phosphorylated GDH1 harmonizes with RSK2 to drive CREB activation and tumor metastasis in EGFR-activated lung cancer. *Cell Rep.* 41, 111827 (2022).
16. Hu, Q. et al. Deacetylation of GLUD1 maintains survival of lung adenocarcinoma cells under glucose starvation by inhibiting autophagic cell death. *Cell Insight* 3, 100186 (2024).
17. Mooz, J. et al. ARAF suppresses ERBB3 expression and metastasis in a subset of lung cancers. *Sci. Adv.* 8, eabk1538 (2022).
18. Yaeger, R. & Corcoran, R. B. Targeting alterations in the RAF–MEK pathway. *Cancer Discov.* 9, 329–341 (2019).
19. Karoulia, Z. et al. New perspectives for targeting RAF kinase in human cancer. *Nat. Rev. Cancer* 17, 676–691 (2017).
20. Grbovic, O. M. et al. V600E B-RAF requires the HSP90 chaperone for stability and is degraded in response to HSP90 inhibitors. *Proc. Natl Acad. Sci. U.S.A.* 103, 57–62 (2006).
21. Rebocho, A. P. & Marais, R. ARAF acts as a scaffold to stabilize BRAF–CRAF heterodimers. *Oncogene* 32, 3207–3212 (2013).
22. Venkatanarayan, A. et al. CRAF dimerization with ARAF regulates KRAS-driven tumor growth. *Cell Rep.* 38, 110351 (2022).
23. Riegel, K. et al. RAF kinases are stabilized and required for dendritic cell differentiation and function. *Cell Death Differ.* 27, 1300–1315 (2020).
24. Yaeger, R. & Corcoran, R. B. Targeting alterations in the RAF–MEK pathway. *Cancer Discov.* 9, 329–341 (2019).
25. Stelzer, G. et al. The GeneCards suite: From gene data mining to disease genome sequence analyses. *Curr. Protoc. Bioinformatics* 54, 1.30.1–1.30.33 (2016).
26. Tian, Q. et al. RICH1 inhibits breast cancer stem cell traits through activating the Hippo signaling kinase cascade. *Cell Death Dis.* 13, 71 (2022).
27. Charan, J. & Kantharia, N. D. How to calculate sample size in animal studies? *J. Pharmacol. Pharmacother.* 4, 303–306 (2013).
28. Li, Z. et al. Silencing GRHL3 promotes distant metastasis of lung squamous cell carcinoma by enhancing SOX2 stability via SIRT1. *J. Pathol.* 265, 302–315 (2025).
29. Xiong, L. et al. Glutamic-pyruvic transaminase 1 deficiency-mediated metabolic reprogramming facilitates colorectal adenoma–carcinoma progression. *Sci. Transl. Med.* 17, eadp9805 (2025).

ARTICLE IN PRESS

Figure Legends:**Figure 1: Involvement of GLUD1 in Anoikis Resistance and Metastasis of EOC**

(A) Volcano plot of GLUD1 expression in epithelial ovarian cancer (EOC) from GEO datasets. Colors indicate gene expression levels: red for high, blue for low, and grey for non-significant expression changes. (B) Venn diagram illustrating the overlap among DEGs, anoikis-related genes, and amino acid metabolism-related genes. (C) GLUD1 expression in the GSE27651 dataset. Gene expression levels are shown with red representing tumor tissues and blue representing normal controls. (D) Kaplan–Meier curves showing overall survival differences between high and low GLUD1 expression groups in EOC patients from the TCGA dataset. Red and blue lines represent high and low expression levels, respectively. (E) Western blot analysis of GLUD1 expression in OVCAR3 and SKOV3 cells cultured under detached conditions. GAPDH was used as a loading control. (F) Representative immunohistochemistry images (Upper) and quantification (Lower) of GLUD1 expression in para-tumor, primary, and metastatic EOC tissues. (G) Overall survival curve and disease-free survival curve for EOC patients with low or high expression of GLUD1 based on IHC staining index. Data are presented as mean \pm SD.

* $p < 0.05$, ** $p < 0.01$.

Figure 2. GLUD1 Dysregulation Drives Anoikis Resistance and Migration in EOC Cells.

(A) Western blot analysis of GLUD1 expression in ovarian cancer cells with GLUD1 overexpression or knockdown. (B) Representative fluorescence images of live (green) and dead (red) cells under detached conditions (left) and quantification of live dead cell ratios (right). (C) Flow cytometric analysis of apoptosis in ovarian cancer cells cultured under detached conditions and corresponding quantification. (D) Transwell migration assays of SKOV3 and OVCAR3 cells

with GLUD1 overexpression or knockdown and quantification of migrated cells. (E) Wound healing assays assessing migratory capacity of SKOV3 and OVCAR3 cells and quantification of wound closure. All experiments were performed in three independent biological replicates. Data are presented as mean \pm SD. * $p < 0.05$, ** $p < 0.01$, *** $p < 0.001$.

Figure 3. GLUD1 inhibition suppresses peritoneal dissemination in vivo (A) Establishment of an intraperitoneal ovarian cancer implantation mouse model. (B) Survival curves of tumor bearing mice injected with control or GLUD1 silenced cells. (C) Representative images of peritoneal metastatic nodules. (D) Quantification of metastatic nodules per mouse. (E) Representative images of H&E, Ki-67, and TUNEL staining of tumor tissue sections. (F) Quantification of Ki 67 positive cells and TUNEL positive cells. $n = 6$ mice per group. Data are presented as mean \pm SD. * $p < 0.05$, ** $p < 0.01$.

Figure 4. GLUD1 interacts with ARAF and activates MEK/ERK signaling (A) Mass spectrometry analysis identifying candidate GLUD1 interacting proteins in GLUD1 overexpressing cells. (B) Peptide spectra supporting the interaction between GLUD1 and ARAF. (C) Co immunoprecipitation analysis of GLUD1 and ARAF in cells expressing the indicated cells. (D) Immunofluorescence images showing the subcellular localization of GLUD1 and ARAF with mitochondrial staining. Scale bars, 20 μm . (E) Western blot analysis of ARAF, MEK, phosphorylated-MEK, ERK, phosphorylated-ERK, BCL-2, BIM, cleaved-caspase 3 in the indicated cells. GAPDH was used as a loading control. (F) Western blot analysis showing rescue of ARAF expression and ERK activation by ARAF re-expression in GLUD1 silenced cells. (G) Time course analysis of ARAF and MEK/ERK signaling under detached conditions in ovarian

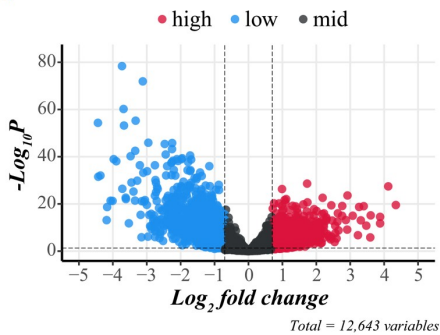
cancer cells. GAPDH was used as a loading control.

Figure 5. GLUD1 Stabilizes ARAF by Suppressing Ubiquitin Proteasome Mediated

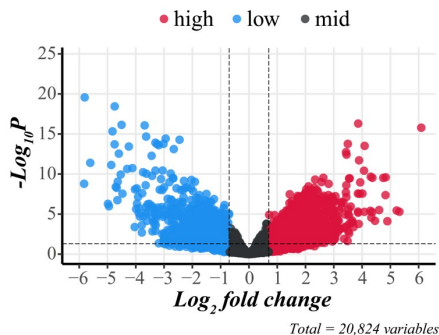
Degradation. (A) Western blot analysis of ARAF protein levels in cells treated with the proteasome inhibitor MG132. (B) Western blot analysis of ARAF protein levels in GLUD1-silenced cells treated with cycloheximide (CHX; 25 $\mu\text{g}/\text{mL}$) for 0, 4, 8, and 12 hours (left). The decay curve of ARAF, normalized to GAPDH and to the 0-hour time point, is shown on the right. (C) Immunoprecipitation of ARAF followed by immunoblotting for ubiquitin to assess ARAF ubiquitination in the indicated cells. (D) Live dead cell staining of detached ovarian cancer cells following GLUD1 knockdown with or without ARAF re-expression and quantification. (E) Transwell migration assays assessing the effects of ARAF re expression on migration of GLUD1 silenced cells and quantification. Data are presented as mean \pm SD from three independent experiments. * $p < 0.05$, ** $p < 0.01$, *** $p < 0.001$, **** $p < 0.0001$.

Figure 6. GLUD1 expression correlates with ARAF in clinical EOC specimens (A)

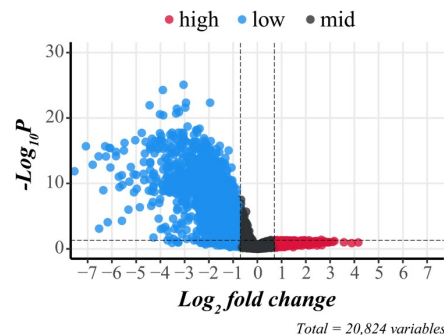
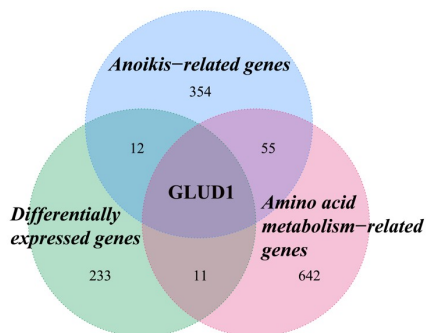
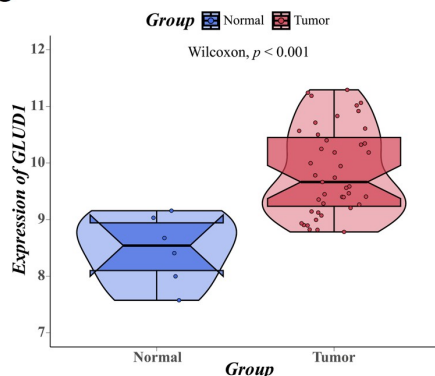
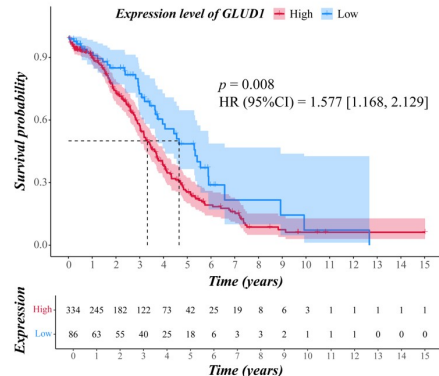
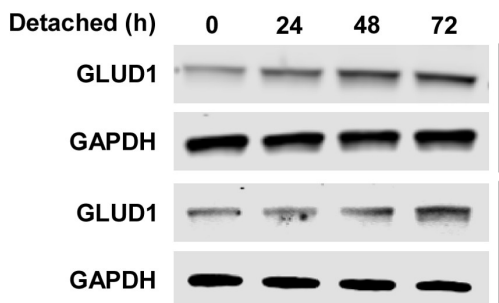
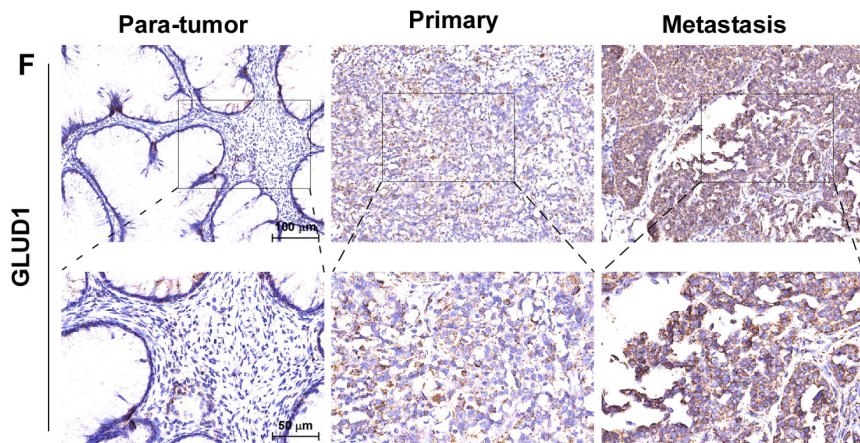
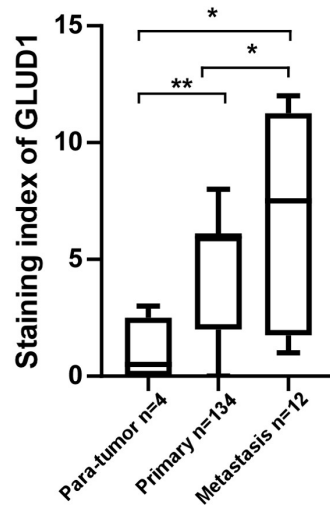
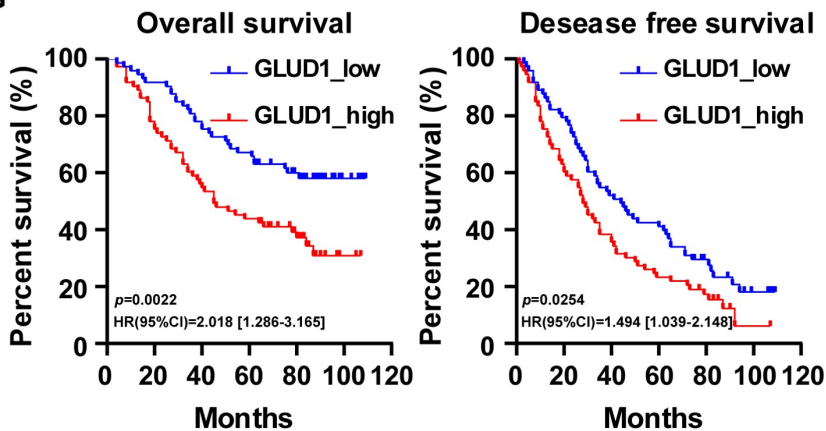
Representative immunohistochemical (IHC) staining images of GLUD1 and ARAF in EOC tissues (left). Correlation analysis of GLUD1 and ARAF protein expression levels in clinical EOC samples (right). (B) Western blot analysis of GLUD1 and ARAF in 10 freshly collected EOC tissue samples (left). Linear regression analysis demonstrating their correlation (right). (C) Schematic model illustrating GLUD1 mediated stabilization of ARAF and activation of MEK/ERK signaling to promote anoikis resistance and metastatic dissemination in EOC.

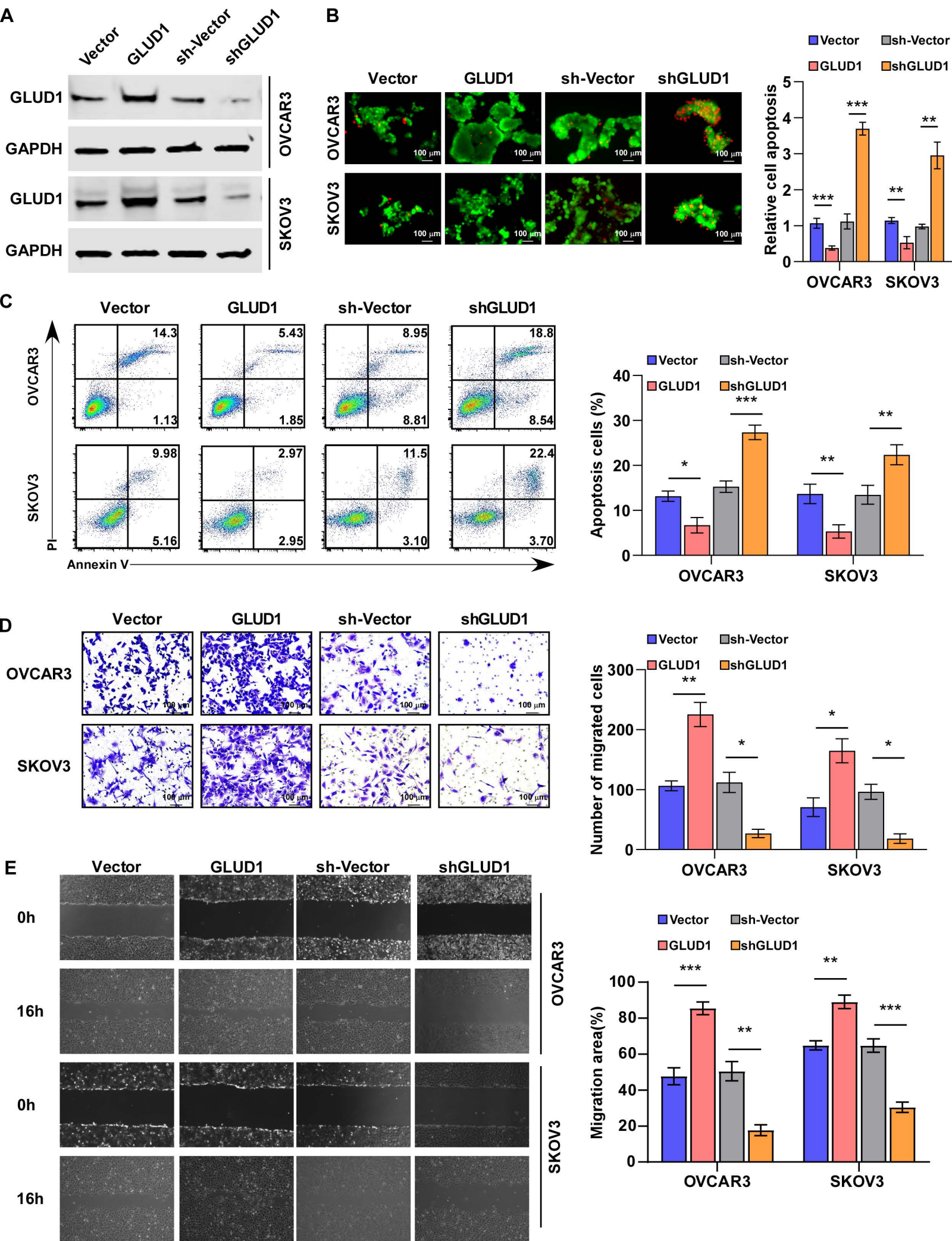
A Differential expression analysis of GSE26712

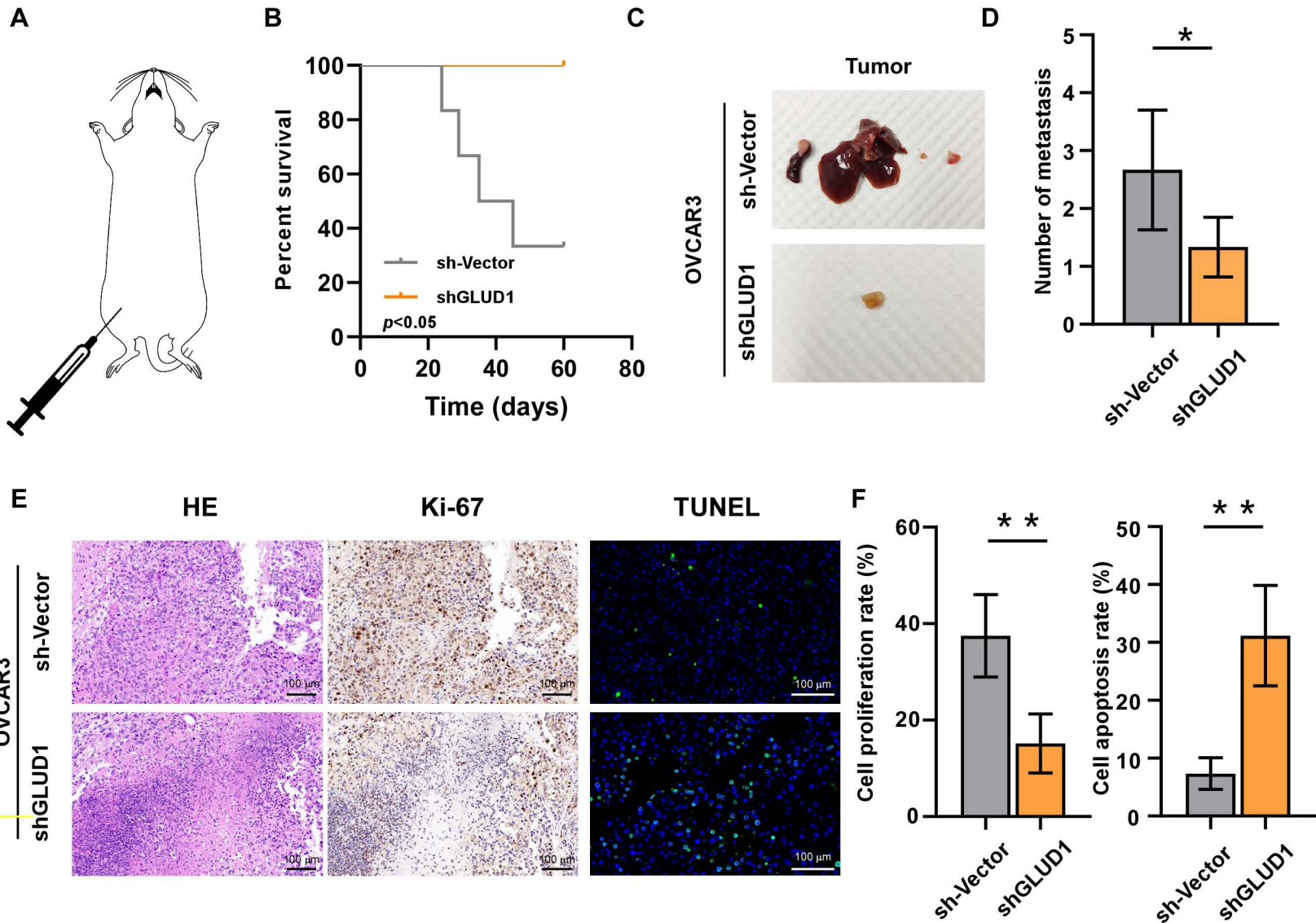
Differential expression analysis of GSE27651

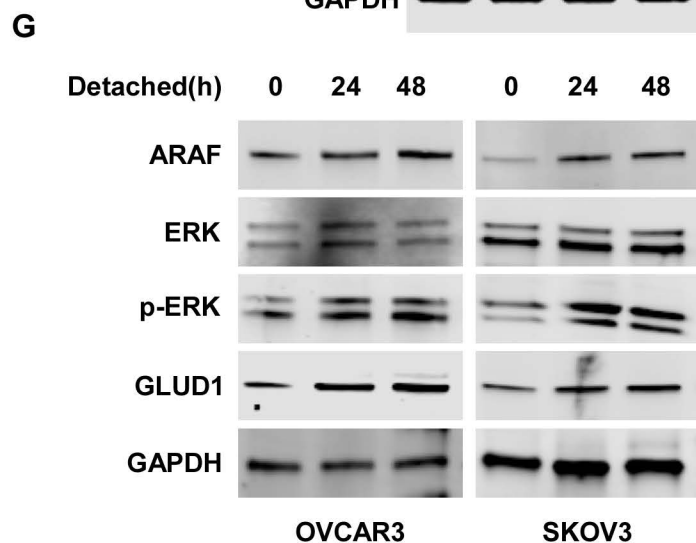
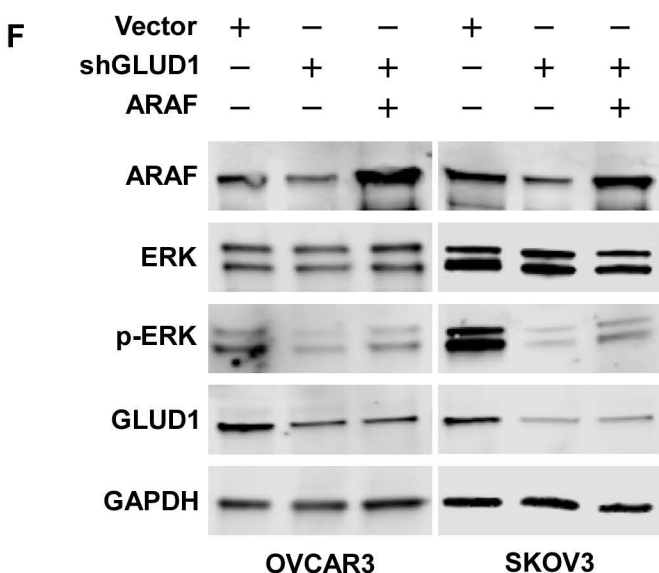
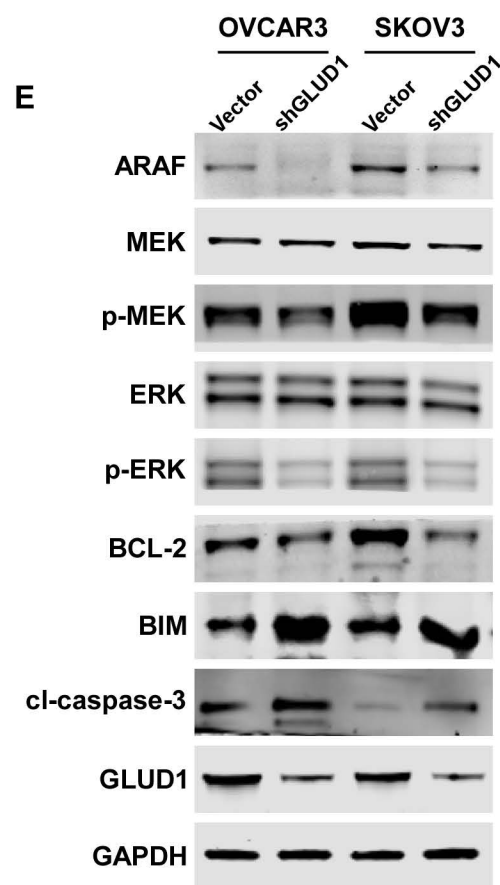
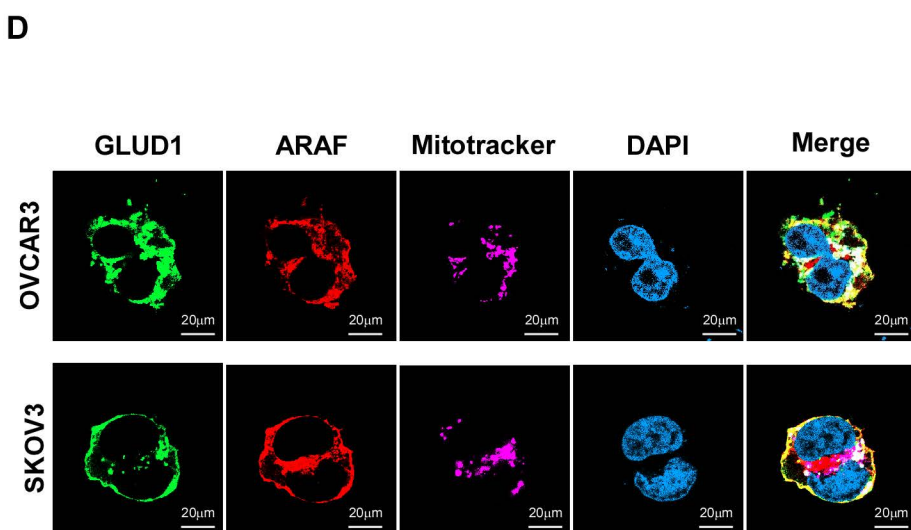
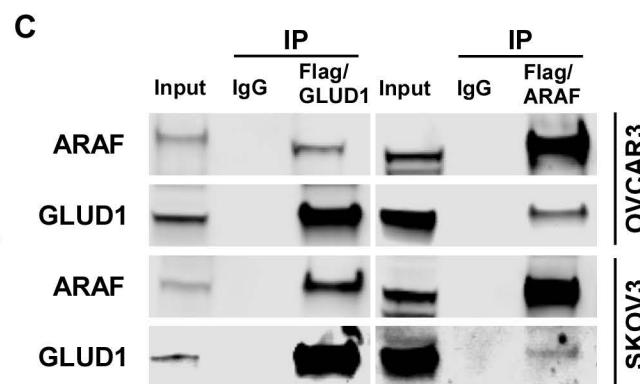
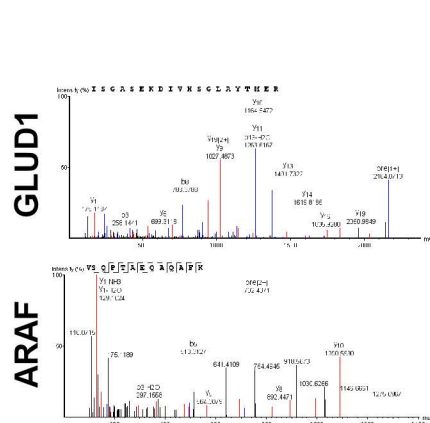
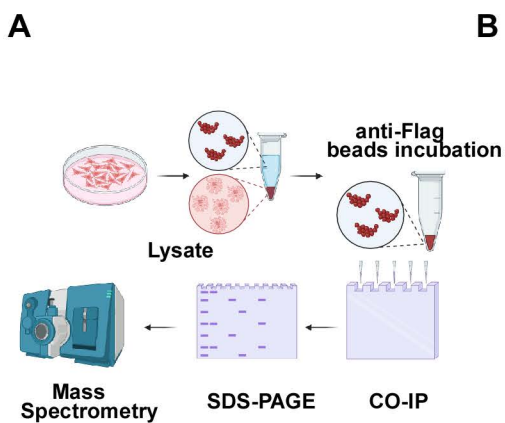


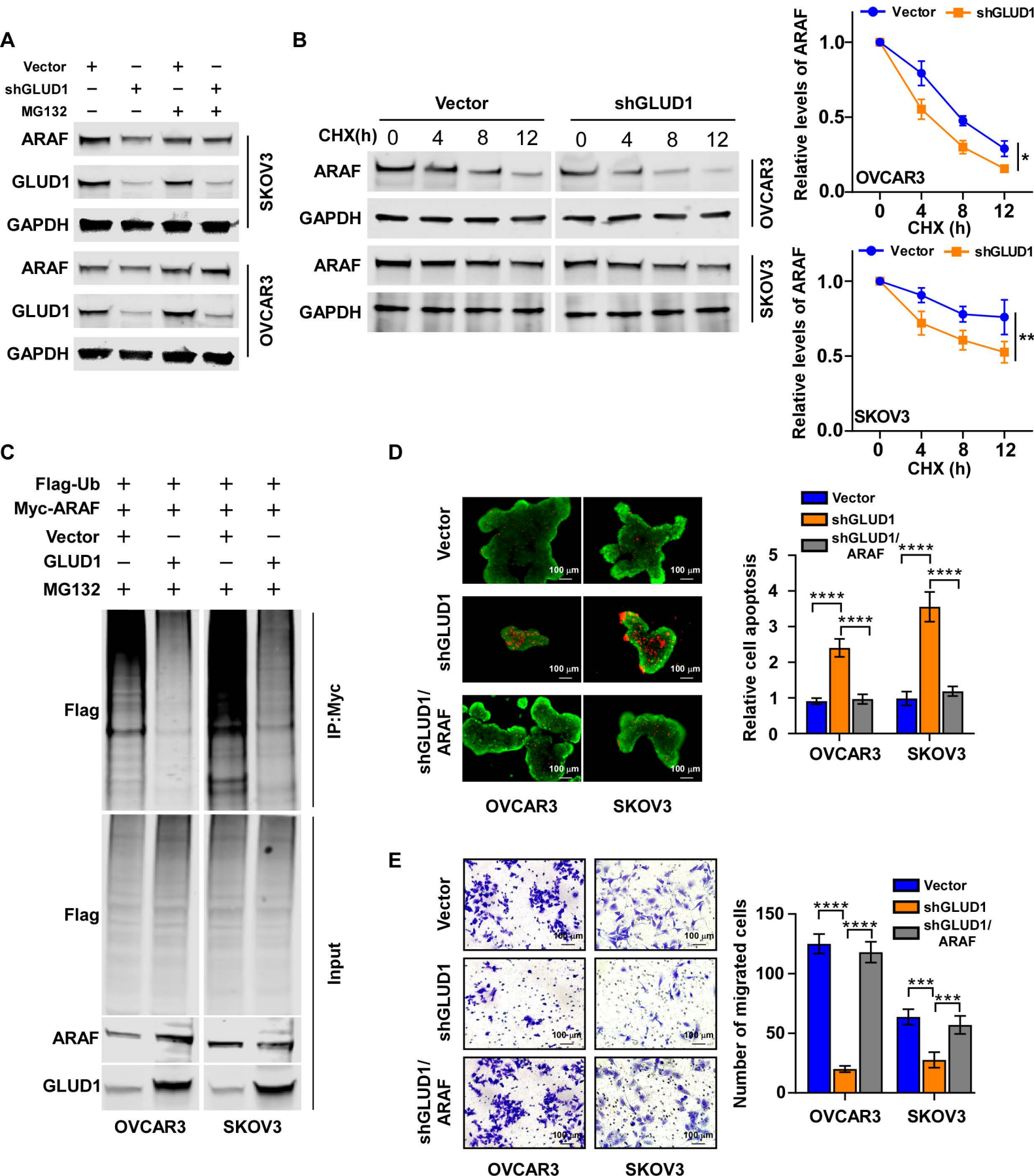
Differential expression analysis of GSE40595

**B****C****D****E****F****G**

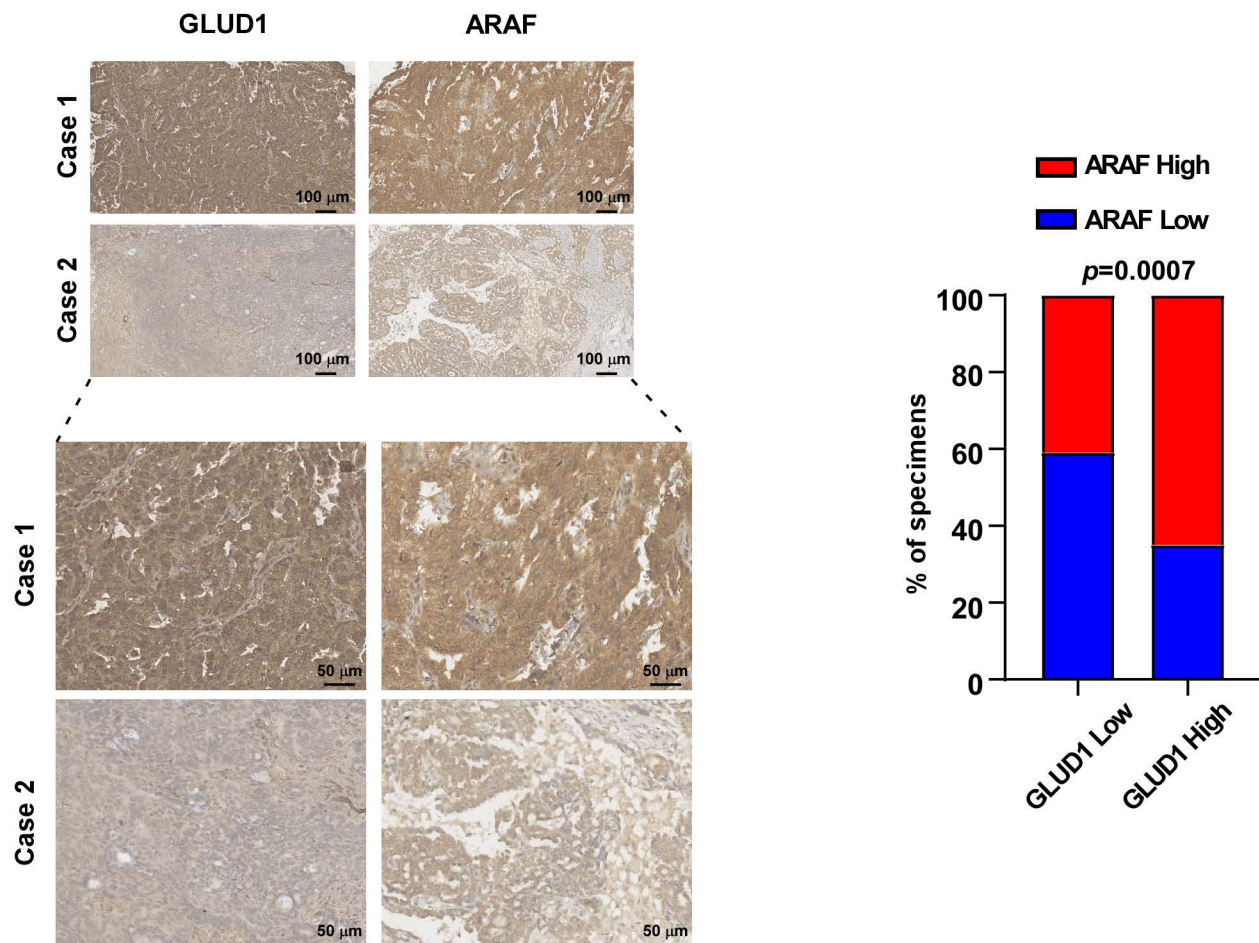




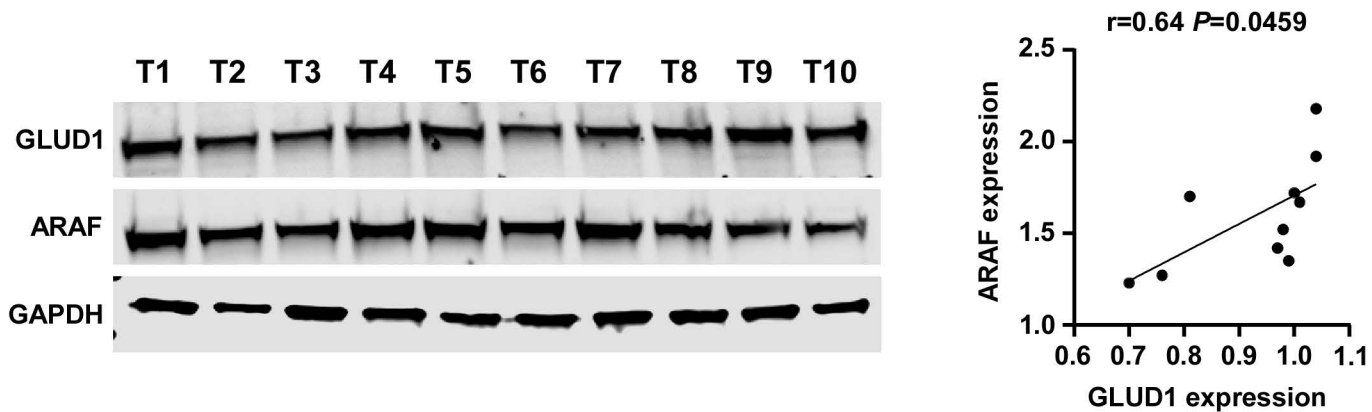




A



B



C

